The Planetary Science Journal, 1:19 (6pp), 2020 June https://doi.org/10.3847/PSJ/ab8f34

Catastrophic Disruption of Hollow Ice Spheres

Kathryn H. Harriss and Mark J. Burchell
Centre for Astrophysics and Planetary Science, School of Physical Sciences, University of Kent, Canterbury, Kent, CT2 7NH, UK; m.j.burchell@kent.ac.uk
Received 2020 February 6; revised 2020 April 21; accepted 2020 April 21; published 2020 June 2

Abstract

Catastrophic disruption is a possible outcome of high-speed collisions in the solar system. The critical energy density Q^* (impact energy/mass of the target), which is taken to mark the onset of catastrophic disruption, occurs when the largest intact fragment post-impact is 50% of the original target mass. Studies of Q^* usually suppose the target body is a solid, rigid object. However, what if the body has a rigid shell and a hollow interior? Here, hollow ice spheres (a diameter of 19–20 cm with an ice thickness of 2.5–3.6 cm) were impacted at speeds up to ~5 km s^{-1}. Catastrophic disruption occurred at $Q^* \sim 25.5 \pm 0.5$ J kg^{-1}, greater than that for similar size solid, or water-filled ice spheres (16–18 J kg^{-1}). However, while the Q^* value has increased, the actual impact energy associated with the new value of Q^* has not, and the change in Q^* arises due to the lower mass of the hollow target bodies.

Unified Astronomy Thesaurus concepts: Impact phenomena (779); Jovian satellites (872); Saturnian satellites (1427)

Supporting material: animation

1. Introduction

Impact speeds between solar system bodies depend on their orbital speed around the local dominant mass body (often the Sun, but for a satellite in a bound orbit, it can be a nearby larger mass object such as a planet) as well as the mutual self-gravitational attraction. The outcome is a speed often measured in units of km s^{-1} (see for example, Hughes & Williams 2000 or Zahnle et al. 2003). Such impacts generate extreme shocks (with peak pressures of 10–100 s of GPa) because the speed of compression waves in the materials involved are themselves typically just a few km s^{-1}. Given that smaller bodies are much more frequent in the solar system than larger ones, the usual outcome is an impact-cratering event on the larger (target) body. However, if the impact energy density Q (defined as the impactor kinetic energy divided by the mass of the combined target-projectile system; note, however, that the impactor mass is relatively so small it is often neglected in this calculation) is too great, the target body can break apart in a catastrophic disruption process. Further, if there is sufficient residual energy, the parts can disperse against their self-gravity.

The critical threshold value of Q that results in the largest single surviving fragment having a mass 50% of the target parent mass is called Q^* and is taken as marking the onset of catastrophic disruption (see Fujiwara et al. 1989 for a discussion). The value of Q^* for a given target body can be found via experimentation for small bodies in the laboratory, where target strength dominates. Extrapolation to larger sizes is required, however, partly because bodies become weaker as their size increases (initially lowering Q^*). Then, for target bodies above approximately a few 100 m in radius, the energy needed to disperse the target fragments against their self-gravity (preventing re-accumulation as a rubble pile object) becomes dominant, resulting in an increasing Q^* as the target size increases (see Holsapple 1993). Other factors such as obliquity of impact, porosity of the target, etc., can also influence Q^* (e.g., Stewart & Leinhardt 2009; Leinhardt & Stewart 2012). Hydrocode simulations are often used to predict Q^* values (e.g., Benz & Asphaug 1999), but the need to compare to real data via laboratory experimentation remains. Laboratory experiments also permit the introduction of new conditions into the impacts—for example. spinning targets (Morris & Burchell 2017).

Although, in the inner solar system, rock is a major component of bodies, ice is also present in many bodies in the outer solar system. There have therefore been many studies on disruption of icy bodies, with calculations ranging from hydrocode simulations (e.g., Benz & Asphaug 1999) to analytic models (e.g., Leliwa-Kopystyński et al. 2016) and many laboratory experiments (e.g., Arakawa 1999; Ryan et al. 1999; Burchell et al. 2005; Leliwa-Kopystyński et al. 2008; Yashui et al. 2014; Shimaki & Arakawa 2012).

However, while most models of catastrophic disruption consider the target as a body of uniform composition (e.g., solid ice), nature often arranges matters differently in the solar system. Recent interest in icy bodies in the outer solar system has included the so-called ice-ocean worlds of Enceladus, Europa, Titan, Ganymede, and Callisto (see Hendrix et al. 2019 for a discussion). Technically, the term ocean world includes the Earth, but by adding the prefix "ice," this implies the body also has a substantial ice component. The usual image of an ice-ocean world is thus of a body with an icy surface and an interior ocean. The liquid does not have to be water, however, and Titan also has areas of liquid hydrocarbons on its surface. For astrobiological purposes, water is of more interest, however, and in the cases of Enceladus (Hansen et al. 2006) and Europa (Sparks et al. 2016), there is evidence via plumes, of connection between the interior oceans and the external surrounding space. Leaving aside the astrobiological interest, however, another question arises—namely, how do such worlds respond to impact processes? Large impactors may penetrate the surface ice, or even cause disruption, limiting the

lifetime of the body in its current state. Laboratory studies have shown how the presence of a subsurface layer of differing composition can influence crater growth (e.g., see Harriss & Burchell 2017 for a discussion on cratering in ice over differing substrates including water). Similarly, numerical studies have considered—for example, how to penetrate the Europan crust (Turtle & Pierazzo 2001) or how the impact-induced shock can propagate through an ice-ocean world and influence the shape of the rocky core (Monteux et al. 2016).

As stated above, if impacts are sufficiently energetic, compared to the mass of the target, the result of an impact will be the catastrophic disruption of the target body. While this might not be a serious hazard for icy satellites today, over the lifetime of the solar system the flux of potential impactors is sufficient that the smaller satellites (such as Enceladus) are at risk, particularly if the period of Late Heavy Bombardment is considered (Movshovitz et al. 2015). In that work however, the Q^* values for icy bodies were estimated assuming they were solid ice. The question of survival of ice-ocean worlds (with liquid, subsurface oceans) against catastrophic disruption has been considered in laboratory experiments (Burchell et al. 2020). They, surprisingly, showed that for ice shells of some 18–19 cm in diameter, with an ice crust thickness of 4 cm and with interiors filled with water, Q^* remains unaltered (16.15 ± 1.35 J kg^{-1}) when compared with that for a solid ice sphere of a similar diameter (18.0 ± 0.7 J kg^{-1}). Although this result suggests that, at least in the strength regime, the approach of Movshovitz et al. (2015) to calculating Q^* as if a body were solid ice reasonable, it does not address the issue of the relative roles of the core and the surface layers in determining the outcome of the impact. Previous work on cratering has shown that this layering does influence cratering growth. This has been shown in both modeling work and experiments on semi-infinite targets (e.g., Senft & Stewart 2007; Stickle & Schultz 2012, 2013; Burchell et al. 2015 and Harriss & Burchell 2017). Indeed, it has been shown via modeling that on semi-infinite targets, the presence of a surface layer of thickness comparable to the projectile can absorb up to 70% of the impact energy (Stickle & Schultz 2012). This in turn raises the question of which is more important in catastrophic disruption of a layered body—the crust or the core? In this current work, we therefore explore this question by constructing hollow ice shells and observing what is needed to catastrophically disrupt them.

2. Method

The hollow ice shells were made using purified water, which was then boiled immediately before use. Once boiled, it was rapidly cooled by standing it in a container with initially liquid water running over its surface and then with crushed ice placed against the container. We have previously shown that preparing water like this, followed by freezing, produces ice with few internal bubbles or stress (e.g., see Figure 1 in Shrine et al. 2002). The water was then pumped into a rubber balloon in a pre-shaped spherical mold (made of two hemispheres, with an internal diameter of 19–20 cm). This assembly was then placed in a freezer at −23°C. A slow freezing process then occurred from the surface of the balloon inward with a liquid core remaining. The thickness of the ice was dictated by the duration of the freeze. After a set time (here 30 hr), the ice crust thickness was found to be 30 ± 5 mm. The ice sphere was then removed from the freezer, the interior water was drained from the ice target via a small hole at the top of the ice sphere, and the balloon material removed from the exterior surface. This resulted in a hollow ice shell. A typical target is shown in Figure 1. Some surface blemishes were seen on the exterior of the ice sphere after removal of the balloon material, but these were small-scale features. The ice spheres were examined before use for signs of interior cracks or flaws, and any such targets were rejected. The hole at the top of the sphere was typically <1 cm in diameter, and in the experiments, it was not found to act as a particular locus for fractures or cracks.

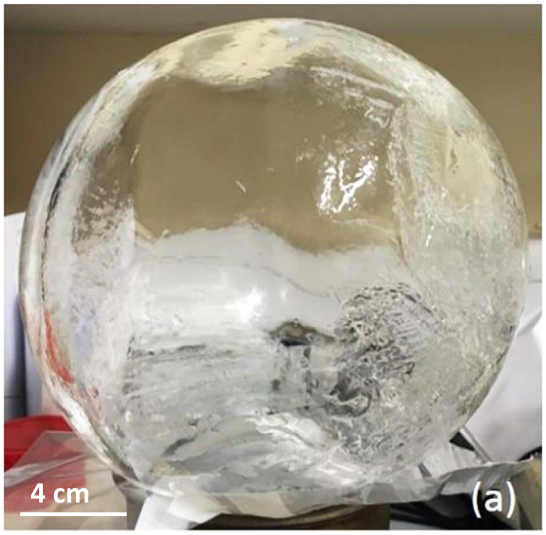

Figure 1. Typical ice target pre-shot.

The ice shell was then placed as the target in a two-stage light gas gun at the University of Kent (Burchell et al. 1999). The target chamber was evacuated to a low pressure of 50 mbar during a shot to prevent deceleration of the projectile in flight. The projectile used was a 1.5 mm diameter glass sphere, whose speed in flight was measured (to better than 1%) by its passage through two light curtains of known separation. Impacts were at normal incidence. After a shot, the target was removed from the gun and examined. Targets were imaged during the impact using a Panasonic HXWA30 camera, and a typical series of frames is shown in Figure 2 for a disrupted target.

Eleven shots were carried out at speeds ranging from 2.2 to 5.1 km s^{-1} (see Table 1). The results were categorized as cratering, penetration, or disruption. In the intermediate case of penetration, the ice shell was still a single rigid structure, but the crater that formed during the impact penetrated into the interior of the shell. Crater diameters were measured along four equally spaced diameters across the crater and were then averaged; the uncertainty given on the diameter is the standard deviation of the four individual measurements. The ice shell thickness varies slightly across the sphere, and the value given is that near the impact point. The crater depth was measured after the impact and is given as calculated from the original ice sphere surface, i.e., by taking the depth below the exposed surface after impact and by adding the thickness of ice above that surface that was removed during the impact (see Leliwa-Kopystyński et al. 2008). All target masses were measured before each shot using a scale sensitive to better than 1 g. The ice target mass pre-shot (m_i) is given in Table 2, along with the mass of the largest ice fragment post-shot (m_f; plus the next three largest fragments) and the ratio m_f/m_i. For cratering and penetrating shots, the largest ice fragment post-shot is the shell

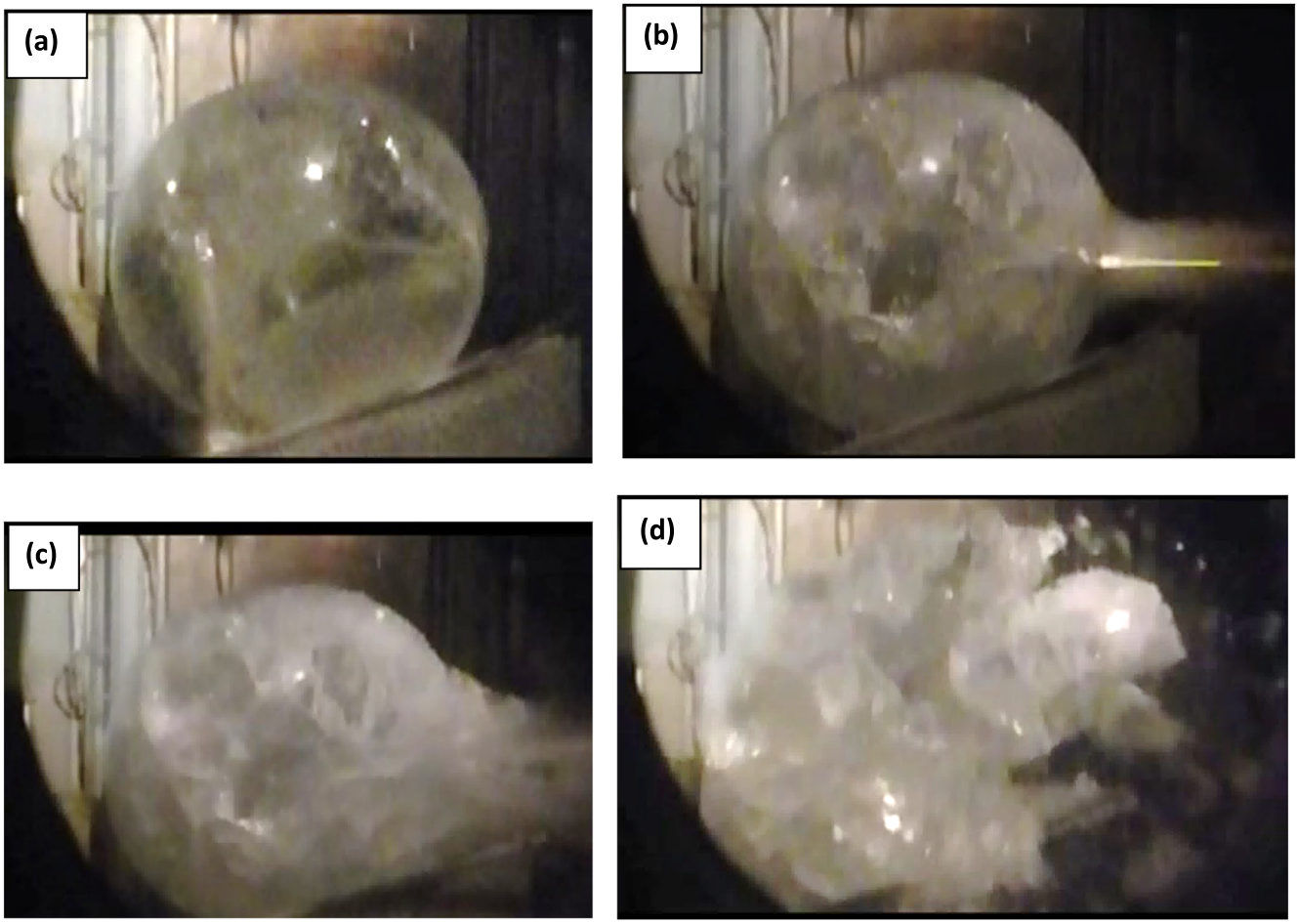

Figure 2. Disruption of a target. Four frames are shown from a high-speed video of an impact at 5.03 km s^{-1}. The impact was from the right. (a) Pre-impact, $t = 0$ s (b) $t = 17$ ms, the initial ejecta can be seen from the impact point, along with a light flash; (c) $t = 191$ ms, the heavily shattered target is starting to move apart while the ejecta from the impact site is now well developed; and (d) $t = 1720$ ms, the target fragments are now separating and moving outward. Note the impact was not at $t = 0$ but occurred between frames (a) and (b). In (b), it can be seen that even while the initial ejecta is being removed from the impact site, the whole ice shell is already fractured. In (d), the large ice fragments from the broken shell are now moving apart. The complete video is available online. The images were taken at 120 frames per second, and the sequence is played back twice, with the second iteration at a much slower frame rate.

(An animation of this figure is available.)

itself (the missing ice is absent from the impact crater). For the disrupted cases, the post-shot mass is that of the largest single ice fragment recovered from the target chamber.

3. Results

In Table 1, no crater diameter exceeds 43% of the diameter of the total ice sphere. The maximum diameter can be compared to the largest craters observed in similar experiments on solid ice spheres, 82% (Leliwa-Kopystyński et al. 2008), or water-filled ice spheres, 70% (Burchell et al. 2020). Also in Table 1, it can be seen that the maximum crater depth observed was 74% of the ice shell depth without penetrating the ice. This compares to 62% for water-filled ice spheres. The various timescales for disruption can be seen in Figure 2. The initial ejecta from the impact site is coincidence in time with the initial fracturing of the whole target. The disassembly of the target then occurs on a longer timescale. In Figure 2(b), a light flash can be seen emerging as a plume from the impact point. Impact light flashes on ice have been observed before in the laboratory (e.g., Burchell et al. 1996), and indeed flashes and radiant plumes have been observed from controlled impacts on icy solar system bodies such as comets (A'Hearn et al. 2005; Schultz et al. 2007).

In Figure 3(a), the ratio m_f/m_i is plotted versus Q. for targets where the ice thickness was approximately 24–31 mm (average 28.5 ± 2.9 mm). In Figure 3, the error bars on each datum are negligible, as the projectile velocity was measured to better than 1% and the masses were measured to a similar accuracy. Taking the traditional definition of Q^* as the value of Q where $m_f/m_i = 0.5$, we can see that $Q^* \sim 25.5 \pm 0.5$ J kg^{-1}. This compares to Q^* for solid ice spheres of (18.0 ± 0.7 J kg^{-1}) and (16.15 ± 1.35 J kg^{-1}) for water-filled ice spheres. There is clearly a significant difference in Q^* for catastrophic disruption of a hollow ice sphere compared to filled or solid ice bodies.

In the case here when the ice layer is some one-third of the overall target radius, the Q^* value is 1.5 times that for a solid body (either solid ice or water-filled ice). If, in the case of the water-filled ice spheres, all the energy went into disrupting the surface ice, the removal of the interior water would leave the energy required for disruption unchanged. However, this would cause a reduction in the target mass to two-third of the mass compared to the totally solid target case and hence a ×1.5 increase in Q^* compared to the solid target case—which is what

Table 1
Details of the 11 Impact Experiments and Their Outcomes

Speed (km s^{-1})	Ice Shell Thickness (mm)	Crater Diameter (mm)	Crater Diameter/Ice Target Diameter	Crater Depth Measured from the Original Surface (mm)	Crater Depth/Shell Thickness	Outcome
2.22	35.7	75.0 ± 8.9	0.375 ± 0.045	17.5	0.74	Crater
3.31	33.1	54.0 ± 2.9	0.270 ± 0.014	⋯	⋯	Penetration
3.84	31.0	85.2 ± 4.4	0.426 ± 0.022	n.r.	n.r.	Crater
4.29	35.7	78.5 ± 9.2	0.392 ± 0.046	⋯	⋯	Penetration[a]
4.50	35.0	⋯	⋯	⋯	⋯	Disruption
4.55	25.0	54.4 ± 2.3	0.272 ± 0.011	10.2	0.61	Crater
4.78	28.5	⋯	⋯	⋯	⋯	Disruption
4.90	30.1	⋯	⋯	⋯	⋯	Penetration[a],[b]
4.92	24.2	⋯	⋯	⋯	⋯	Disruption
5.03	36.0	⋯	⋯	⋯	⋯	Disruption
5.08	30.1	⋯	⋯	⋯	⋯	Disruption

Notes. Note that for the shot at 3.84 km s^{-1}, the crater depth was not recorded (marked n.r.). Possible outcomes are Crater (where the impact crater is fully contained in the ice shell), Penetration (where a crater is seen, but there is a hole in the crater floor into the interior of the target), and Disruption (where the target broke into multiple fragments after impact). Where the impact penetrated the ice or disrupted the target, no crater depth is given, as it is by definition unknown.
[a] These targets had multiple fractures throughout.
[b] Target fell apart during handling so it was not possible to measure the crater.

is observed. This implies that it is the interaction in the thick surface ice layer that causes disruption, irrespective of the presence of a core (water or more ice).

This would imply that as the ice layer becomes thicker, the data would converge toward that for a solid ice target. This is tested in Figure 3(b), where the original data are shown along with that for the thicker ice targets (an ice thickness of 33–36 mm with an average of 35.1 ± 1.2 mm), i.e., on average 23% thicker. At small Q values, the resulting crater still forms as before in the ice layer. At larger Q values, when disruption has occurred, the data has shifted leftward on Figure 3(b) compared to that for the thinner ice (implying a lower Q^* value), moving toward the range expected for a solid ice target.

Thus the catastrophic energy density Q^* for a thick shell hollow body can be found by taking Q^* for a solid body of similar density and increasing it proportional to the inverse of the reduction in mass due to its hollow nature. Then, as the ice shell gets thinner, at some minimal shell thickness, we suggest that the impactor will penetrate before sufficient energy is transferred to the shell, causing regional, rather than global, damage and a sudden change in Q^* as the simple relationship displayed here fails. Exploration of this latter point is left for future work.

4. Discussion

The problem posed here is a somewhat artificial one. Unlike the case of ice bodies with interior oceans, a hollow ice sphere has no known planetary science analog. The results do permit us, however, to explore the role of the shell versus interior in catastrophic disruption of thick-shelled targets. As Q increases toward Q^*, there is increasing damage in the surface ice shell. However, as noted in the Section 3, the maximum observed crater diameter in the case just below catastrophic disruption did not reach the same fraction of the sphere diameter that it does for solid or water-filled ice spheres. This is possibly linked to the penetration that occurs into the interior of the target, which is observed before the onset of catastrophic disruption. In previous work on water-filled ice spheres, the onset of surface layer penetration was accompanied by the appearance of large radial (tensile) fractures in the surface ice layer (Burchell et al. 2020). This was also seen here, and as Q increased further, these radial cracks in the surface occurred around most of the target and were accompanied by increasing shear damage, initially near the impact site but then across increasingly large regions of the target. The target then finally failed catastrophically as Q was increased to Q^*.

In previous work on semi-infinite layered targets, with ice over various substrates, for impact speeds of around 5 km s^{-1} and 1.5 mm diameter projectiles (the same size as used here), the target behaved as semi-infinite when the ratio t_R (surface layer thickness/projectile diameter) exceeded around 15 (Harriss & Burchell 2017). In that earlier work, penetration into the substrate only occurred when the value of t_R fell below 7. For $7 < t_R < 15$, the surface layer was not penetrated, but the resultant crater was narrower than expected in a semi-infinite ice target. Here for impact speeds in the range 4–5 km s^{-1}, we find that penetration has occurred even though t_R is approximately 20–22. This suggests that the absence of an underlying layer is significant in terms of crater growth and penetration.

In the literature, there is discussion on the transition from cratering to penetration in plates of various thicknesses as the target thickness changes. For the example of aluminum and Teflon targets, it is reported that the onset of penetration is associated with rear surface spallation beneath the impact point (Horz 2012). Thus it is not the crater growing so deep that it penetrates the surface layer, which causes the transition from cratering fully in the surface layer to penetration into the interior. Similarly in the literature, for cases just above the transition to penetration, there is no trace of the projectile reported beneath the target (Horz 2012), suggesting that the projectile itself is still fully contained in the surface layer in such cases.

It is worth noting that here, as previously when impacts on water-filled ice spheres of the same size were reported, it was observed that shock-induced damage to the surface ice layer had spread around the sphere while the impact crater was still forming (Burchell et al. 2020). Thus the timescale of damage occurring in the shell is not observed to change significantly with the presence/absence of a filled interior.

Table 2
Mass of Target Fragments Post-shot

Speed (km s^{-1})	Q Impact Energy Density (J kg^{-1})	m_i Ice Shell Mass Pre-shot (kg)	m_f Mass of Largest Ice Fragment Post-shot (kg)	Mass of Second Largest Fragment (kg)	Mass of Third Largest Fragment (kg)	Mass of Fourth Largest Fragment (kg)	m_f/m_i
2.22	4.75	2.294	2.228	…	…	…	0.9712
3.31	10.4	2.320	2.234	…	…	…	0.9629
3.84	12.8	2.613	2.548	…	…	…	0.9750
4.29	16.7	2.444	2.112	…	…	…	0.8642
4.50	22.5	1.993	0.267	0.187	0.179	0.121	0.1340
4.55	21.6	2.120	2.000	…	…	…	0.9434
4.78	24.9	2.033	1.077	0.1688	0.077	…	0.5296
4.90	21.5	2.512	2.163	…	…	…	0.8611
4.92	27.3	1.966	0.256	0.240	0.229	0.094	0.1302
5.03	20.3	2.727	0.308	0.179	0.120	0.108	0.1129
5.08	25.9	2.206	0.188	0.125	0.114	0.107	0.0852

Note. The post-shot largest fragment mass was either the mass of the ice shell (with a crater in it), or, if disrupted, the mass of the largest ice fragment. The impact energy density Q is the impact kinetic energy divided by the original mass of the target. Where the target was disrupted by the impact, the mass of the four largest fragments are given, ordered by decreasing mass.

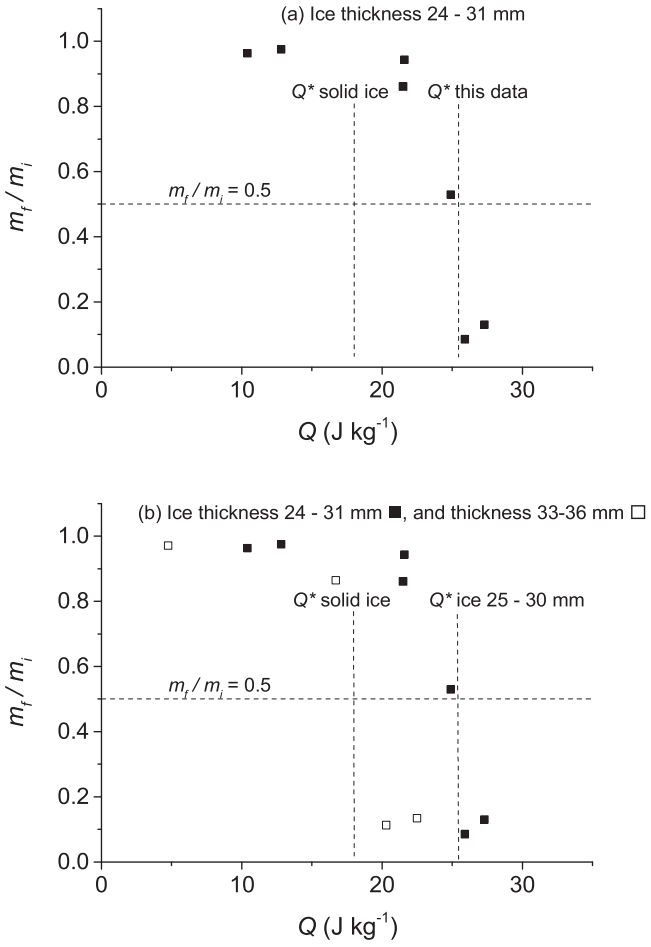

Figure 3. Fractional mass of largest intact fraction post-shot vs. Q. (a) For targets with ice thickness 24–31 mm. (b) Same as (a) but with four thicker ice (33–36 mm) targets. The horizontal dashed line shows $m_f/m_i = 0.5$, which gives Q^*. The vertical dashed line shows Q^* for solid ice targets and that obtained here.

As stated in Section 1, it has previously been reported that in layered targets, the surface layer can absorb up to 70% of the impact energy, even if t_R has a value if just 1 or 2 (Stickle & Schultz 2012). Given that here we have much greater t_R values, we should expect the large majority of the impact energy to be coupled to the surface shell of ice, even in cases where penetration into the interior has occurred. (Until penetration, or significant rear surface spallation occurs, all the impact energy, by definition, remains coupled into the ice shell except that removed by the crater ejecta). This energy is then available to shatter the ice layer. Yet it remains that 1.5 times the energy is needed to shatter a given mass of ice when it is arranged in a hollow shell shape compared to when it is a solid sphere. Either the geometry is playing a significant role, with the absence of shock wave propagation through the interior being important, or once penetration has occurred, an increase in Q results in the escape from the shell into the interior of a significant portion of the impact energy. Given the previous observations about how well impact energy couples into even relatively thin surface layers, it would seem the former point is more likely, i.e., that shock transmission through the core of a body is important when causing disruption. Note a subtle point, however: the shell has still been damaged early in the process even if the core is hollow. It is the physical breaking apart of the shell that seems more difficult to achieve without a core.

The known ocean worlds with ice shell exteriors seem in lie in two categories: those with relatively thin shells, e.g., Europa, where the ice thickness is typically estimate to be of order 1% of the body radius (see Peddinti & McNamara 2019 for a recent discussion), and those with thick shells, e.g., Enceladus, where estimates of the ice thickness range from 7% to 35% of the body radius (Thomas et al. 2016; Lucchetti et al. 2017). The latter case is comparable to the experiments here (where the ice thickness is 25%–38% of the radius of the body). Here, however, there is a hollow interior. If there is interest in failure of hollow shells, then thick shell hollow spheres are found to be susceptible to catastrophic disruption from an impact of similar energy to that which would cause disruption in a filled target of same size and density, and Q^* can be predicted accordingly. The fate of thin shell spheres against impact is still to be explored. It would also be instructive to take targets with surface layers of fixed thicknesses and vary the projectile size to see how that changes the outcome.

We thank STFC (UK) for funding this work and M. Cole for firing the light gas gun.

ORCID iDs

Mark J. Burchell https://orcid.org/0000-0002-2680-8943

References

A'Hearn, M. A., Belton, M. J. S., Delamere, W. A., et al. 2005, Sci, 310, 258
Arakawa, M. 1999, Icar, 142, 34
Benz, W., & Asphaug, E. 1999, Icar, 142, 5
Burchell, M. J., Cole, M. J., McDonnell, J. A. M., et al. 1999, MeScT, 10, 41
Burchell, M. J., Cole, M. J., Ramkissoon, N. K., et al. 2015, M&PS, 50, 1436
Burchell, M. J., Cole, M. J., & Ratcliff, P. R. 1996, Icar, 122, 359
Burchell, M. J., Landers, K., Harriss, K. H., et al. 2020, Icar, 336, 113457
Burchell, M. J., Leliwa-Kopystynski, J., & Arakawa, M. 2005, Icar, 179, 274
Fujiwara, A., Cerroni, P., Davis, D. R., et al. 1989, in Asteroids II, ed. R. P. Binzel, T. Gehrels, & M. Shapley Matthews (Tucson, AZ: Univ. Arizona Press), 240
Hansen, C., Esposito, L., Stewart, A. I. F., et al. 2006, Sci, 311, 1422
Harriss, K. M., & Burchell, M. J. 2017, M&PS, 52, 1505
Hendrix, A. R., Hurford, T. A., McEwan, A. S., et al. 2019, AsBio, 19, 1
Holsapple, K. A. 1993, AREPS, 21, 333
Horz, F. 2012, M&PS, 47, 763
Hughes, D. W., & Williams, I. P. 2000, MNRAS, 315, 629
Leinhardt, Z. M., & Stewart, S. T. 2012, ApJ, 745, 79
Leliwa-Kopystyński, J., Burchell, M. J., & Lowen, D. 2008, Icar, 195, 817
Leliwa-Kopystyński, J., Włodarczyk, I., & Burchell, M. J. 2016, Icar, 268, 266
Lucchetti, A., Pozzobon, R., Mazzarini, F., et al. 2017, Icar, 297, 252
Monteux, J., Collins, G. S., Tobie, G., et al. 2016, Icar, 264, 300
Morris, A. J. W., & Burchell, M. J. 2017, Icar, 296, 91
Movshovitz, N., Nimmo, F., Korycansky, D. G., Asphaug, E., & Owen, J. M. 2015, GeoRL, 42, 256
Peddinti, D. A., & McNamara, A. K. 2019, Icar, 329, 251
Ryan, E. V., Davis, D. R., & Giblin, I. 1999, Icar, 142, 56
Schultz, P. H., Eberhardy, C. A., Ernst, C. M., et al. 2007, Icar, 190, 295
Senft, L. E., & Stewart, S. T. 2007, JGR, 112, E11002
Shimaki, Y., & Arakawa, M. 2012, Icar, 218, 737
Shrine, N. R. G., Burchell, M. J., & Grey, I. D. S. 2002, Icar, 155, 475
Sparks, W. B., Hand, K. P., McGrath, M. A., et al. 2016, ApJ, 829, 121
Stewart, S. T., & Leinhardt, Z. M. 2009, ApJ, 691, L133
Stickle, A. M., & Schultz, P. H. 2012, JGR, 117, E07006
Stickle, A. M., & Schultz, P. H. 2013, M&PS, 48, 1638
Thomas, P. C., Tajeddine, R., Tiscarno, M. S., et al. 2016, Icar, 264, 37
Turtle, E. P., & Pierazzo, E. 2001, Sci, 294, 1326
Yashui, M., Hayama, R., & Arakawa, M. 2014, Icar, 233, 293
Zahnle, K., Schenk, P., Levison, H., et al. 2003, Icar, 163, 263